

15-state R -matrix investigation of resonances in the inelastic scattering of electrons from atomic hydrogen at energies up to 13.06 eV

W. C. Fon and K. Ratnavelu

Department of Mathematics, University of Malaya, 59100 Kuala Lumpur, Malaysia

K. M. Aggarwal*

Department of Applied Mathematics and Theoretical Physics, The Queen's University of Belfast, Belfast, BT7 1NN, Northern Ireland

(Received 19 April 1993; revised manuscript received 23 August 1993)

A 15-state R -matrix calculation has been carried out at 530 energies ranging from the $n=2$ threshold up to $n=5$ threshold at 13.06 eV to map out the resonant profiles for the $n=2$ inelastic integral and differential cross sections, and the angular distribution of the spin asymmetry in the inelastic scattering of spin-polarized electrons by the spin-polarized hydrogen atoms at angles 0° , 30° , 55° , 70° , 90° , 125° , and 180° for the $1s \rightarrow 2s$ transition. The calculations are compared with the experiments and the feasibility studies of using the electron-energy-loss experiments in the investigation of resonances with positions higher than the $n=2$ threshold have been carried out.

PACS number(s): 34.80.Dp, 34.80.Nz

I. INTRODUCTION

Williams [1] reported electron-impact excitation of resonances between the principal quantum number $n=2$ and 3 states of atomic hydrogen by observation of radiation from the spontaneous decay of the $2p$ state and from the delay quenching of the $2s$ state in an external field. Integral excitation cross sections for the $2s$ and $2p$ states were measured separately over the energy range from about 10.2 to 12.08 eV with an electron energy resolution quoted to be 9 meV. From the measurements on the energy dependence of optical excitation functions for the $2s$ and $2p$ states, he found (i) a rich cluster of resonances; many of these were observed for the first time. Wherever comparison is possible, the extracted resonant positions were reported to be in excellent agreement with the calculation of Callaway [2]. However, at electron energies converging to the $n=3$ threshold, the optical functions show complicated and irregular structure which makes extraction of resonant positions and widths almost impossible. This cannot be explained by cascade effects as there is a complete absence of cascades in this energy range. (ii) There is considerable similarity between the structure in the $2s$ and $2s+2p$ integral cross sections and it is only the depths or the heights of the structure that were appreciably different (see Fig. 1).

Measurements of optical excitation functions do not permit the classification of resonances. The identification of resonances and extraction of resonant positions and widths from excitation functions becomes complicated when resonances are close together and contributions from overlapping resonances in partial waves from differing (L, S) symmetries are combined. Consequently, the true structure is masked by interference and it gives

rise to irregular features in the excitation functions. One way to tackle this problem was suggested by Andrick, Ehrhardt, and Eyb [3] by using electron scattering measurements. As a resonance is mainly associated with one particular partial wave, angular distribution analysis of the corresponding differential cross sections (DCS) opens up the possibility of choosing suitable scattering angles so that one or more of these resonances is suppressed due to the zeros of the corresponding Legendre polynomials (see Table I). In this way, closely packed resonances of different symmetries can be discerned and positions and widths of the resonances extracted separately (see Fon and Lim [4]).

Measurements on the angular distribution (as a function of electron energy) of those electrons which have lost 10.2 eV in exciting either the $2s$ or $2p$ state were first reported by Williams [5] at scattering angles of 30° , 60° , and 90° . The observed spectra change dramatically with angle. A clear interpretation of angular behavior of the resonance state was difficult and the values of resonant positions and widths were also not given. This was attributed to the following problems. (i) The electron energy resolution was not high enough to resolve the details of the resonant profile. (ii) The $2s$ and $2p$ states' contributions were not separated in electron-energy-loss experiments so the spectra presented corresponded to the sum of the individual differential cross sections. The mixing of $2s$ and $2p$ cross sections in the $n=2$ spectra might have contributed to the irregular feature of the resonant profile.

Warner, Rutter, and King [6] repeated the electron-energy-loss experiments with better electron energy resolution and overall improvement in sensitivity and performance. A clear interpretation of angular behavior of the resonance state was still found difficult. Only a few resonant positions were extracted and no classification of resonance symmetries was given. However, they found reasonable agreement in the positions and shapes of the resonance features between the observed differential cross

*Permanent address: Department of Physics and Astrophysics, University of Delhi, Delhi 110007, India.

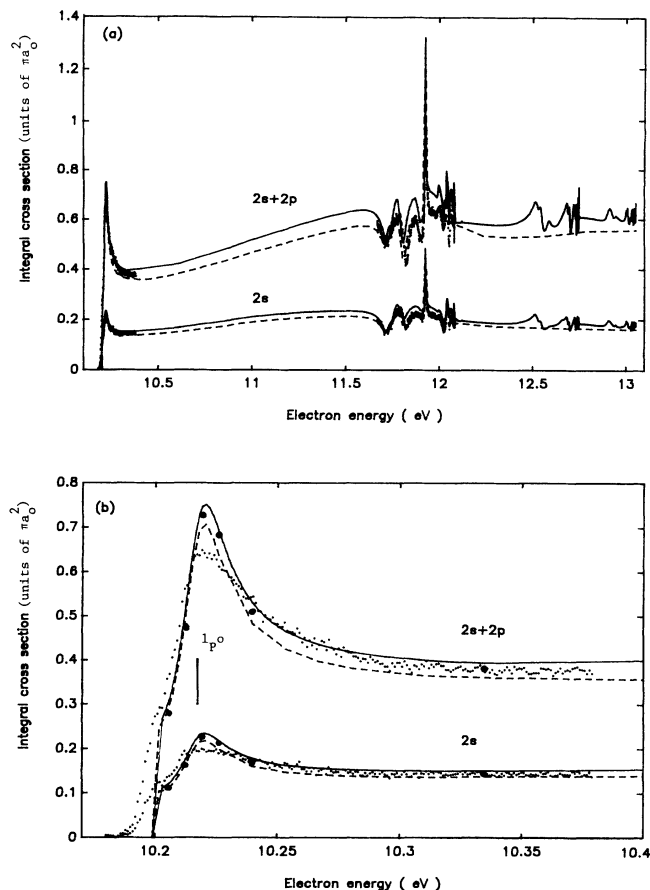


FIG. 1. Integral cross section (units of πa_0^2) for the $1s \rightarrow 2s$ and $1s \rightarrow 2s + 2p$ transitions is shown as a function of the incident electron energy. The experimental points are those of Williams [1]. The full curves are the theoretical values of the 15-state R -matrix calculation and the dashed curves are the calculation of Callaway [2]. The closed circles (\bullet) are the calculation of Taylor and Burke [22].

sections and the calculation of Morgan, McDowell, and Callaway [7] if the calculated values were convoluted with a Gaussian function of 25 meV full width at half maximum (FWHM) to allow for the energy spread of the incident electron beam. In particular, at scattering angle 90° , the agreement was more striking and the prominent peak featuring the ${}^3F^o$ resonance was completely suppressed by both theoretical and experimental curves. One would expect this to happen only if the $2s$ cross sec-

TABLE I. Electron scattering angles specially chosen to suppress resonances of particular symmetries as the corresponding partial waves vanish due to the zeros of Legendre polynomials.

θ	Type of resonances expected to be suppressed
30°	${}^{2S+1}G^\pi$
55°	${}^{2S+1}D^\pi, {}^{2S+1}H^\pi$
70°	${}^{2S+1}G^\pi$
90°	${}^{2S+1}P^\pi, {}^{2S+1}F^\pi, {}^{2S+1}H^\pi$
125°	${}^{2S+1}D^\pi, {}^{2S+1}H^\pi$

tion were separated out for consideration. This might indicate that the structure of the $2s$ DCS is similar to those of the $2s + 2p$.

It is extremely difficult to separate the $2s$ and $2p$ states in experimental DCS measurements. One possibility would be to measure the scattered electron in coincidence with the $2p$ decay photons as demonstrated by Williams [8] at 54.4 eV. The use of such a coincidence technique would, however, lead to much smaller signal counting rates. It is an extremely difficult experiment and even more so if it were to be carried out at low energies and it should be avoided at all cost while there are other alternatives to study the resonance features; for example, the optical technique by observing the radiated photons. However, if the structure of $2s$ DCS were to be similar to those of the $2s + 2p$, there would be no need to separate the $2s$ from the $2p$ states in experimental DCS measurements. The electron-energy-loss experiments will remain as an attractive alternative.

In this paper, the 15-state R -matrix calculations of Pathak and co-workers [9] have been extended to calculate the $n=2$ inelastic integral and differential cross sections and the spin asymmetry in the inelastic scattering of spin-polarized electrons by the spin-polarized hydrogen atom for the $1s \rightarrow 2s$ transition. The aims of this paper are (i) to reconfirm the observation of resonances reported by Williams [1] and Warner, Rutter, and King [6]; (ii) to verify the conservation of similarity in shape between structure of $2s$ and $2s + 2p$ in the DCS measurements; (iii) to probe the sensitivity of the spin asymmetry for $1s \rightarrow 2s$ transition in response to the presence of resonances. The work described in this paper is part of a continuing effort to study resonances in electron scattering from atomic hydrogen in the various decay channels and follows from the work of Fon and co-workers [10] and Pathak and co-workers [9].

II. THE CALCULATION

The R -matrix method for electron-atom collisions has been discussed in detail by Burke, Hibbert, and Robb [11]. The collision calculations are carried out in LS coupling using the R -matrix package of Berrington *et al.* [12]. The target wave functions, energy levels, and scattering wave functions used in the present 15-state R -matrix calculation have been fully described by Pathak, Kingston, and Berrington [9] and Aggarwal *et al.* [13]. However, to recapitulate, the wave function describing the two-electron scattering system can be expanded as

$$\psi_k = \sum_{i,j} a_{ijk} \Phi_i u_j(r) + \sum_j b_{jk} \phi_j, \quad (1)$$

where Φ_i are the channel functions formed from the target states of the hydrogen atom, u_j are the radial basis functions describing the motion of the scattered electron (the continuum orbitals), and ϕ_j are the two-electron functions (the bound-bound orbitals) which allow for short-range correlation effects. These bound-bound orbitals are also designed to represent the target states of the singly ionized atom, coupled to two bounded elec-

trons simulating the possible formation of two-electron resonances.

In theory, if the summation in (1) included all the bound states of the hydrogen exactly and also included an integration over the continuum states of hydrogen then the results would be exact. However, in practice we can only include a small number of target states in (1). In this calculation, only the 15 lowest atomic states ($n = 1, 2, 3, 4,$ and 5) were used in the summation (1) and we did not allow for ionization channels. The R -matrix boundary radius was taken to be 83 a.u. and 48 continuum orbitals were used for each channel angular momentum. At all energies $k^2 \leq 1.02$ Ry, the calculations were limited to partial waves with angular momentum $L \leq 9$ only. At $k^2 = 1.21$ Ry, a few more higher partial waves were needed to ensure convergence. The T -matrix elements for these higher partial waves were obtained by extrapolation.

As there are no pseudostates involved in this calculation, the 15-state R -matrix calculation gives exact excitation thresholds for $n \leq 5$. The use of exact interchannel couplings gives rise to a spectrum of two-electron resonances whose positions and widths are in excellent agreement with the prediction of Gailitis and Damburg [14,15], Callaway [2], Lipsky, Anania, and Conneely [16], Oberoi [17], and Ho and Callaway [18,19] (see [9]). By not including target states where $n \geq 6$, the 15-state R -matrix calculation cannot give information on the resonances occurring beyond the $n = 5$ threshold.

The spin asymmetry as a function of scattering angle θ is defined as

$$A_{i \rightarrow j}(\theta, k_i^2) = (1 - r_{ij}) / (1 + 3r_{ij}), \quad (2)$$

where r_{ij} is the ratio of triplet to singlet cross section for the $i \rightarrow j$ transitions.

III. RESULTS AND DISCUSSIONS

The 15-state R -matrix calculations of Pathak and co-workers [9] and Fon, Ratnavelu, and Aggarwal [10] have been extended to obtain the differential cross sections and the spin asymmetry $A_{1s \rightarrow 2s}(\theta, k^2)$ for the transitions

$$e^- + \text{H}(1s) \rightarrow e^- + \text{H}(2s + 2p) \quad (3)$$

$$\rightarrow e^- + \text{H}(2s) \quad (4)$$

at 530 energies ranging from $n = 2$ threshold up to $n = 5$ threshold at 13.06 eV in order to depict the detailed resonant structures of the observed profile for the $1s \rightarrow 2s + 2p$ and $1s \rightarrow 2s$ integral and differential cross sections, and the angular distribution of the spin asymmetry $A_{1s \rightarrow 2s}(\theta, k^2)$ as functions of electron energies.

A complete presentation of all the results of these calculations would require publication of a very large table giving the cross sections and the values of $A_{1s \rightarrow 2s}(\theta, k^2)$ as functions of 530 energies. This is impractical. Therefore it has been decided to present here some illustrative results in graphic form. A numerical table of the results by energies at $0^\circ, 30^\circ, 50^\circ, 70^\circ, 90^\circ, 125^\circ,$ and 180° can be obtained on request from the authors [20].

A. The $1s \rightarrow 2s$ and $1s \rightarrow 2s + 2p$ integral cross sections

The success and limitation of the close-coupling approximation have been well investigated since its introduction to atomic physics in the early 1930s. In the energy range under consideration, all the ionization channels are closed and only a few discrete channels are open. The scattering processes are predominated by resonances. It is generally accepted that the coupling of discrete channels is instrumental in the emergence of complicated resonant structure in the cross sections, whereas the continuum effects are not expected to play an important role in the formation of resonances (Burke, Ormonde, and Whitaker [21]). In general, for energy lying below the ionization threshold, close-coupling calculations in which physical target states with increasing principal quantum number n are used, yielding accurate qualitative cross section in the energy range up to the highest threshold explicitly included in the expansion. This phenomenon has been known for some time (see, for example, Taylor and Burke [22] and Burke, Ormonde, and Whitaker [21], who examined the $n = 1$ to 2 transitions in electron-hydrogen scattering). The same observation was made by Berrington and Kingston [23] in electron-helium scattering.

The 15-state calculation on the integral cross section (or its equivalent; collision strengths) was extensively discussed by Aggarwal *et al.* [13]. The effect of virtual excitation to the continuum was fully examined by comparison of the 15-state calculation with those of Callaway [2] and Scholz, Walters, and Burke [24] in which the continuum effects were taken into consideration in distinctly different ways. However, to recapitulate, the present 15-state R -matrix calculation on integral cross sections for $1s \rightarrow 2s$ and $1s \rightarrow 2s + 2p$ excitations is compared in Fig. 1(a) with the experiments of Williams [1] and the theoretical values of Callaway [2]. The fact that there is an excellent agreement between the experiments and the calculation of Callaway [2] and that the 15-state results on integral cross sections differ from the experiments by around 10% leads us to the measure of importance of the continuum effects. This is confirmed by the most recent coupled-channels-optical (6CCO) calculation of McCarthy and Shang [25]. Figures 1 and 2 also show that the matching between the qualitative shape of the 15-state results and the experiments is most impressive. This indicates that the reproduction of the qualitative shape of the observed resonant profile by the 15-state calculation is not undermined by the 10% overestimation in the magnitude of the integral cross sections caused by not including the continuum effects. As the calculations of Callaway [2] and McCarthy and Shang [25] did not include physical target states with quantum number $n > 3$, they are not expected to produce correct resonant profile in the energy range beyond $n = 3$ threshold. If the convergent behavior of the close-coupling expansion on the calculation of integral cross sections observed by Burke and his co-workers [21] and [22] is anything to go by, the present 15-state results are the only calculation to date which gives correct resonant profile on the cross sections in the energy range from $n = 2$ to 5 thresholds [see Fig. 1(a)]. The above conclusion is reached without prejudice

on the convergence of the close-coupling approximation in the calculation of differential cross sections. However, there is sufficient evidence to suggest that this is also true in the case of electron-helium scattering (see Fon, Lim, and Sawey [26]). Bray and McCarthy [27] reported that in their 15CCO6 calculation on spin-dependent observables in electron-sodium scattering, the virtual excitation to the continuum has very little effect at energy 4.1 eV (1 eV below the ionization threshold).

Figure 2 shows the detailed resonant profiles of the $1s \rightarrow 2s$ and $1s \rightarrow 2s + 2p$ excitations as functions of incident energy ranging from 11.66 to 12.1 eV. The theoretical values are not convoluted. The vertical bars represent the positions of the resonances as given in Table II in increasing energies. For visual clarity, the 6CCO calculations [25] are presented as vertical offsets and the vertical increments are given in the brackets. Two important observations are noted: (i) The impressive agreement in details between the shape of the 15-

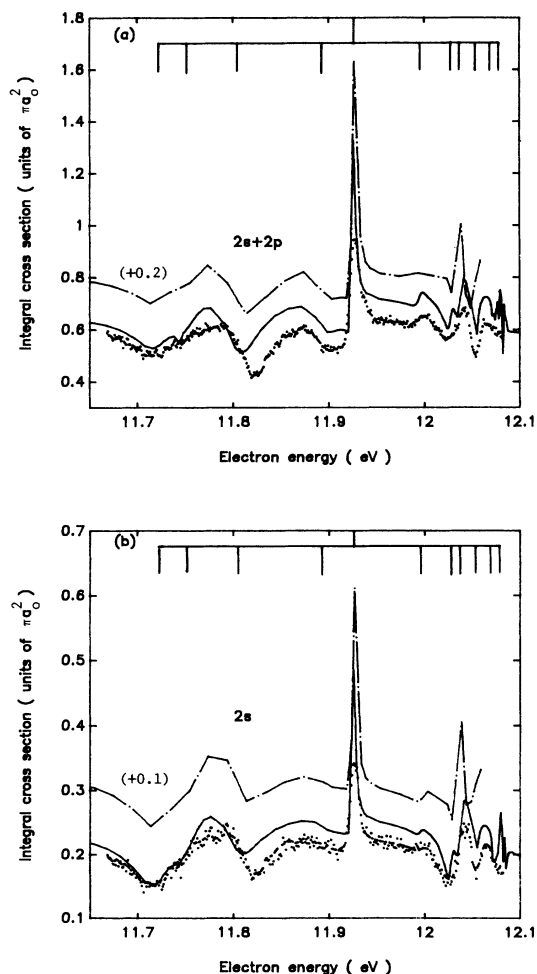


FIG. 2. Integral cross section (units of πa_0^2) for the $1s \rightarrow 2s$ and $1s \rightarrow 2s + 2p$ transitions is shown as a function of the incident electron energy. The curves are the same as in Fig. 1 except the chain curves are the calculations of McCarthy and Shang [25] which are represented as vertical offsets and the vertical increments are given in the brackets. Vertical bars indicate the positions of resonances given in Table II in increasing energies.

TABLE II. Resonant positions and widths.

$2S+1L^\pi$	E_r (Ry)	Γ (10^{-3} Ry)
$^1S^e$	0.861 987	3.01
$^3P^o$	0.864 173	3.43
$^1D^e$	0.868 099	3.14
$^1P^o$	0.874 574	2.51
$^3F^o$	0.876 989	0.228
$^3D^e$	0.882 090	0.772
$^1S^e$	0.884 453	0.580
$^3P^o$	0.885 165	0.607
$^1D^2$	0.886 378	0.428
$^1G^e$	0.887 493	0.952
$^3P^o$	0.888 185	0.113

state results and the profiles of the experiments [1] indicates the convergence behavior of the close-coupling expansion observed by [21] and [22] is indeed correct; (ii) as electron energy moves away from 12 eV and converges to $n = 3$ threshold, the 6CCO calculation [25] does not seem to reproduce the observed structure of the $1s \rightarrow 2s$ and $1s \rightarrow 2s + 2p$ excitation functions. In particular [see Fig. 2(a)], the distinct resonance structure featuring $^3D^e$ resonance at 11.997 eV is absent from the 6CCO calculation [25]. One reason for this could be the fact that the density distribution of energy points used in the calculation is not high enough to portray the complicated structure of the experiments in the energy range where an abundance of closely packed resonances is known to exist. It is important to note that in the study of resonance phenomena, it is the qualitative shape (not the magnitude) of the excitation functions which is of paramount importance here.

One unique feature of the R -matrix calculation is that the accuracy of the calculation is not compromised by the need to obtain results at a large number of energy points (530 energies were used in this paper). This can be accomplished with ease by the R -matrix method (see [11]) and the R -matrix computer package is designed such that 90% of the computer time needed for the calculation is independent of the energy value chosen (see Berrington *et al.* [12]). This makes the 15-state R -matrix calculation ideally suited to the studies of resonance phenomena considered here.

There is considerable similarity between the structure in the $1s \rightarrow 2s$ and $1s \rightarrow 2s + 2p$ excitation cross sections and it is only the depths and the heights that are appreciably different (see Fig. 1). In Fig. 1(b), the theoretical values of Callaway [2] and Taylor and Burke [22] are compared with the present 15-state calculation in the presence of the experimental data of Williams [1] for energies ranging from the threshold to 10.4 eV. The 15-state calculation lies very close to the highly accurate calculation of Taylor and Burke [22] and the calculation of Callaway [2] lies considerably lower than the present calculation. All three calculations exhibit step-function characteristic at the threshold. The shape resonance $^1P^o$ is clearly shown at 0.751 344 eV. The $1s \rightarrow 2s + 2p$ cross sections are seen to differ by a constant factor from those of the $1s \rightarrow 2s$. The arbitrary normalization is interpreted

by Williams [1] as a simple way of showing that the measured data conform to the physical expectation that the resonance just occurs in a single partial wave for both the $2s$ and $2p$ channels and it is the same resonance ${}^1P^o$ at 0.751344 eV in both channels. However, it is not clear how this interpretation can be invoked to explain the similarity between the complicated structure in the $1s \rightarrow 2s$ and $1s \rightarrow 2s + 2p$ excitation cross sections over the energy range shown in Fig. 2.

B. The similarity between the structure in the $1s \rightarrow 2s$ and $1s \rightarrow 2s + 2p$ differential cross sections

Differential cross sections for the excitation of the $n=2$ states were first reported by Morgan, McDowell, and Callaway [7] as functions of energy for angles 30° , 60° , and 90° from 0.85 to 0.8889 Ry. However, the energy spacing used did not appear to be small enough to map out the true structure of the resonant profile and only the rough sketch of the feature was presented graphically. Recently Callaway [28] reported again the $n=2$ excitation differential cross sections. The calculations are a straightforward extension of those reported by Callaway [2]. Eighteen energy points were used to bring out the resonant feature between the $n=2$ threshold and the ${}^3F^o$ resonance at 0.876989 Ry.

To assess the quality of the present R -matrix calculation, Fig. 3 compares the 15-state calculation on $1s \rightarrow 2s$ and $1s \rightarrow 2s + 2p$ DCS's with those of Callaway [28] at 0.877 , 0.81 , and 0.752 Ry with the electron scattering angles ranging from 0° to 180° . The agreement between the two sets of calculations is good. There is remarkable similarity between the shape in the $1s \rightarrow 2s$ and $1s \rightarrow 2s + 2p$ angular distributions with the exception that at energy 0.877 Ry (the ${}^3F^o$ resonance), the depths and the heights of the $1s \rightarrow 2s$ DCS are little more accentuated than those of the $1s \rightarrow 2s + 2p$ excitation reflecting the characteristic of $[P_3(\cos\theta)]^2$.

It may be more convenient to measure the combined cross sections for $n=2$ excitation rather than to separate $2s$ and $2p$ contribution, and to make the measurements with varying energy for fixed scattering angle. In order to verify the conservation of similarity between the structure in the $1s \rightarrow 2s$ and $1s \rightarrow 2s + 2p$ angular distributions, we show results for forward and backward scattering and for angles 30° , 55° , and 90° in Figs. 4–6.

Figure 4 shows the forward and backward scattering cross sections for $1s \rightarrow 2s$ and $1s \rightarrow 2s + 2p$ transitions. We observe exceptionally strong contribution from the ${}^3F^o$ resonance. Other structure is small by comparison. The backward peak for the $1s \rightarrow 2s + 2p$ combined [see Figs. 4(a) and 4(b)] is larger than the forward peak until one is well up into the resonance region. This is primarily a consequence of the fact that the forward maximum in $2p$ excitation is weaker than the backward maximum in the $2s$ [see Fig. 4(d)].

There is striking resemblance of the qualitative shapes between the scattering cross sections for $1s \rightarrow 2s$ and $1s \rightarrow 2s + 2p$ excitations in the forward and backward directions. This is confirmed by the calculation of Calla-

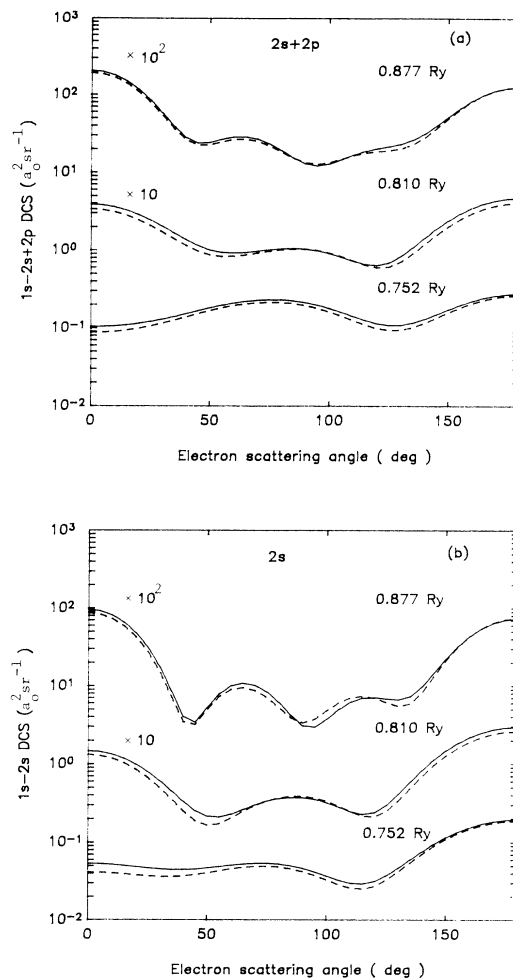


FIG. 3. Differential cross section ($a_0^2 \text{sr}^{-1}$) for the (a) $1s \rightarrow 2s + 2p$ transition; (b) $1s \rightarrow 2s$ transition. Full curves are the theoretical values of the 15-state R -matrix calculation and the dashed curves are the calculation of Callaway [28].

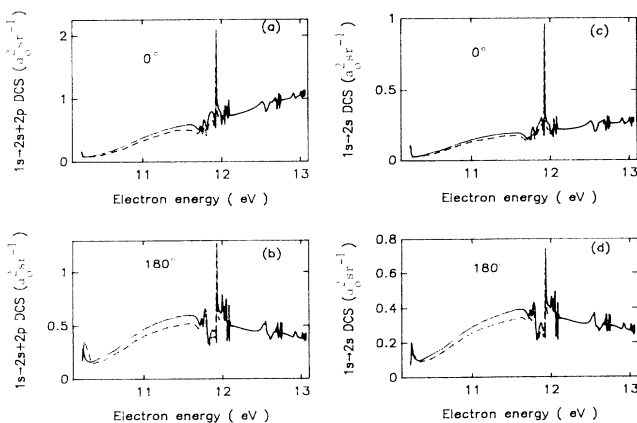


FIG. 4. Differential cross section ($a_0^2 \text{sr}^{-1}$) for the $1s \rightarrow 2s + 2p$ and $1s \rightarrow 2s$ excitations as functions of the incident electron energy from $n=2$ threshold up to $n=5$ threshold at 13.06 eV. The curves are the same as Fig. 3.

way [28]. The similarity in the forward scattering direction is the reflection of the similarity in the structure of the integral cross sections of the same processes reported by Williams [1]. This can be explained by the fact that when $\theta=0^\circ$, $P_l(\cos 0)=1$. The scattering amplitudes in the forward direction for these transitions build up in magnitude "constructively" through the summation over l , while the integral cross sections represent the sum of the individual partial wave contribution. Consequently, the shape of the forward scattering cross sections would be similar to those of the integral cross sections of the same transition, while the depths and heights of the structure may differ. On the other hand, for the backward direction, where $\theta=180^\circ$, $P_l(\cos 180^\circ)=(-1)^l$. The backward scattering amplitudes for both $1s \rightarrow 2s$ and $1s \rightarrow 2p$ excitations represent the difference between the sum of the even partial amplitudes and that of the odd

partial waves.

However, the contributions of resonances may be most readily distinguished at intermediate angles where the energy dependences contrast quite strongly (compare the 55° results for $1s \rightarrow 2s + 2p$ excitation with those for 90° shown in Fig. 5). The shape of the $1s \rightarrow 2s + 2p$ DCS is confirmed by the calculation of Callaway [28]. It is obvious that the profiles of the $1s \rightarrow 2s + 2p$ DCS at 55° and 90° [see Fig. 5] are distinctly quite different from those of the $1s \rightarrow 2s$ DCS [see Figs. 6(b) and 6(c)]. The similarity between the structure in the forward and backward scattering directions of $1s \rightarrow 2s$ and $1s \rightarrow 2s + 2p$ scattering cross sections is not carried over to other intermediate scattering angles. The profile of the $1s \rightarrow 2s + 2p$ DCS is complicated by the mixing between the $2s$ and $2p$ contributions, as the method of choosing suitable scattering angles to suppress resonances of particular symmetry is no longer effective for $s \rightarrow p$ transition. This will be made clear later.

Figure 6 shows the resonant profile of the 15-state R -matrix calculation on $1s \rightarrow 2s$ DCS as a function of energy at scattering angles (a) 30° ; (b) 55° ; (c) 90° ; and (d) 125° . The scattering angles have been chosen to suppress particular resonances as indicated in Table I. The positions of the resonances converging to $n=3$ threshold given in Table II are those of widths broad enough to be observed. It is clear that the ${}^1G^e$ resonance at 0.887493 Ry is suppressed in Fig. 6(a) at scattering angle 30° and the ${}^1D^e$, ${}^3D^e$, and ${}^1D^e$ resonances at energies 0.868099, 0.882090, and 0.886378 Ry are suppressed at scattering angle 55° and 125° [see Figs. 6(b) and 6(d)], while the ${}^3P^o$, ${}^1P^o$, ${}^3F^o$, ${}^3P^o$, and ${}^1P^o$ as indicated in Fig. 6(c) are suppressed at energies 0.864173, 0.874574, 0.876989, 0.885165, and 0.888194 Ry (see Table II). All these match the prediction indicated in Table I.

On the other hand, the $1s \rightarrow 2s + 2p$ DCS shown in Fig. 5 does not seem to conform to the pattern indicated by Table I. At scattering angle 55° , Table I suggests that resonances of the symmetries ${}^{2S+1}D^\pi$ and ${}^{2S+1}H^\pi$ would be suppressed. However, Fig. 5(a) shows that the resonant effects due to the resonances ${}^1D^e$, ${}^3D^e$, and ${}^1D^e$ indicated by long vertical bars are not diminished. Again in Fig. 5(b) at scattering angle 90° , the exceptional large peak due to ${}^3F^o$ resonance at 0.876989 Ry which is expected to completely disappear remains as dominant as ever, while the resonances ${}^3P^o$, ${}^1P^o$, and ${}^3P^o$ whose positions are indicated by long vertical bars are not appreciably suppressed.

The nonconformation of the $1s \rightarrow 2s + 2p$ DCS to the prediction of Table I is due to the mixing between $2s$ and $2p$ contributions in the angular distribution. The $2p$ cross section is more difficult to describe simply because the waves with $L > 0$ are split into two channels corresponding to outgoing angular momentum $l=L+1$ and $l=L-1$. In addition, different angular dependences are associated with the excitation of the $m=0$ and 1 sub-states. We have established that the profile of the $1s \rightarrow 2s + 2p$ DCS, in general, is distinctly different in structure from those of the $1s \rightarrow 2s$ DCS. The mixing of $2s$ and $2p$ contributions in the $1s \rightarrow 2s + 2p$ DCS leads to the destruction of the angular distribution of $1s \rightarrow 2s + 2p$

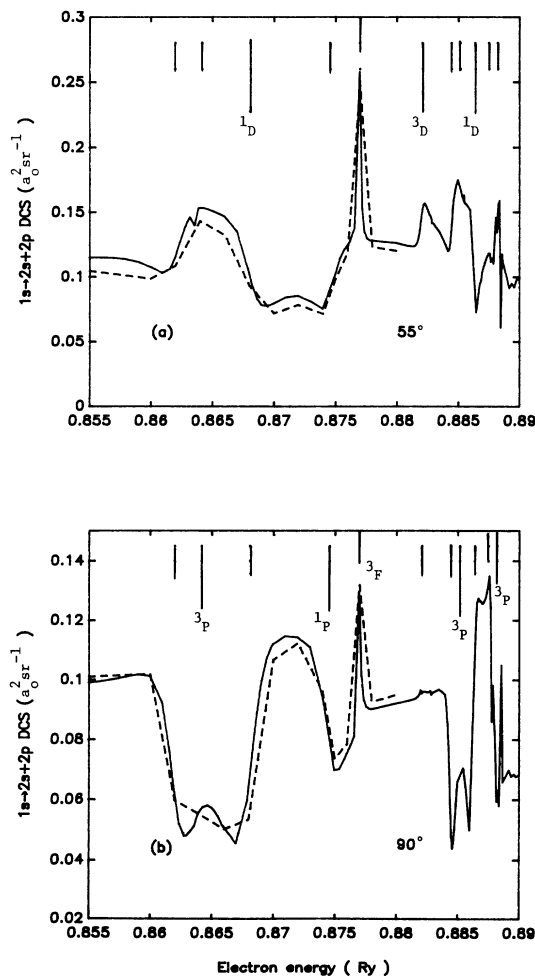


FIG. 5. The 15-state R -matrix calculation of the $1s \rightarrow 2s + 2p$ differential cross section ($a_0^2 \text{sr}^{-1}$) as a function of incident electron energy ranging from 0.855 to 0.89 Ry at scattering angles (a) 55° ; (b) 90° . —, the 15-state R -matrix calculation; ---, the calculation of Callaway [28]. The vertical bars indicate the positions of resonances given in Table II in increasing energies. The long vertical bars with designated symmetries indicate the resonances expected to be suppressed.

excitation being used as a tool to identify resonance symmetry (i.e., the angular momentum and spin of the resonance).

C. Comparison with experiments

Figure 7 compares the 15-state R -matrix calculation on the $1s \rightarrow 2s + 2p$ DCS as a function of energy with the experiments of Warner, Rutter, and King [6] at scattering angles 30° , 55° , 70° , and 90° . The present theoretical values are not convoluted with a Gaussian function of experimental electron energy resolution to emulate the spread of energies in the incident electron beam. The 15-state results represent one of the most detailed calculations to date in terms of sharpness in structure and accuracy. The present qualitative shape and magnitude of the resonant profile for the $1s \rightarrow 2s + 2p$ DCS has been confirmed by the latest calculation of Callaway [28] (see Fig. 5). The experimental excitation functions represent the average of the contributions from the electrons with energy resolution of 25 meV. It is a very difficult experiment. Apart from the low electron energy resolution, the experimentalists also face a host of other problems such as low hydrogen atom-beam density, electron beam

current, and large background contribution from noise at low incident electron energies considered here. The present technology and experimental know-how have not yet permitted the experiments to reproduce the sharp theoretical profile in any degree of close resemblance. Even if they did, the experimental $1s \rightarrow 2s + 2p$ angular distribution would not be in any position to identify the state of the resonances (i.e., the angular momentum and spin of the resonant state) as discussed in Sec. III B.

However, the comparison between the experiments with unresolved resonant features and calculation with sparsely distributed energy points might lead us to wrong conclusions. The calculated 30° and 90° $1s \rightarrow 2s + 2p$ DCS's of Morgan, McDowell, and Callaway [7] are compared in Fig. 2 of the paper [6] with the measurements of Warner, Rutter, and King [6]. The calculated DCS's are also shown in the same figure after convolution with a Gaussian function of 25 meV FWHM to allow for the energy spread of the incident electron beam. The positions and shapes of resonance features in the convoluted DCS of Morgan, McDowell, and Callaway [7] are reported in reasonable agreement with the experiments. In particular, at scattering angle 90° , the calculations before and after convolution do not show a large spike at the posi-

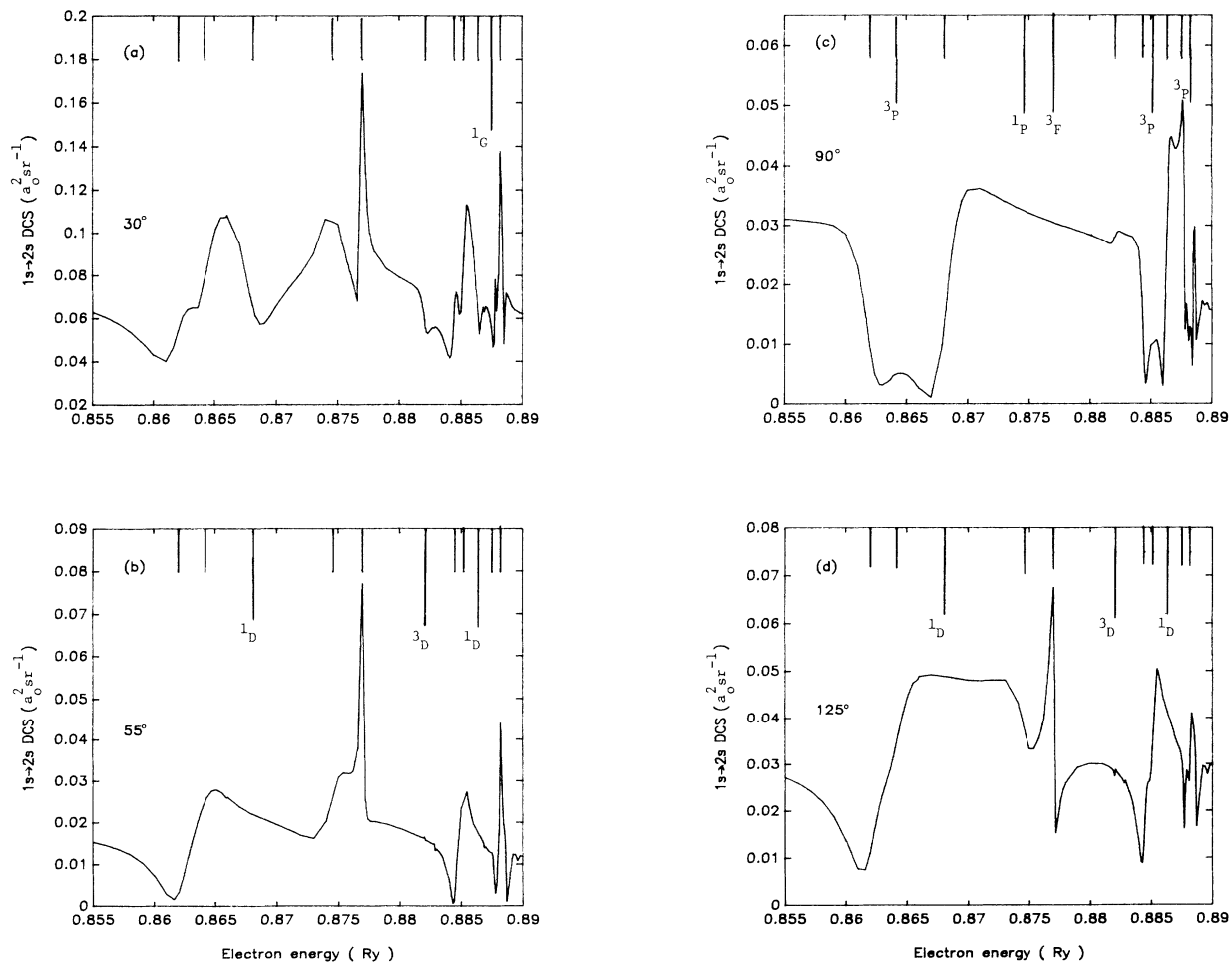


FIG. 6. Same as Fig. 5 except it is for $1s \rightarrow 2s$ differential cross sections and at scattering angles (a) 30° ; (b) 55° ; (c) 90° ; and (d) 125° .

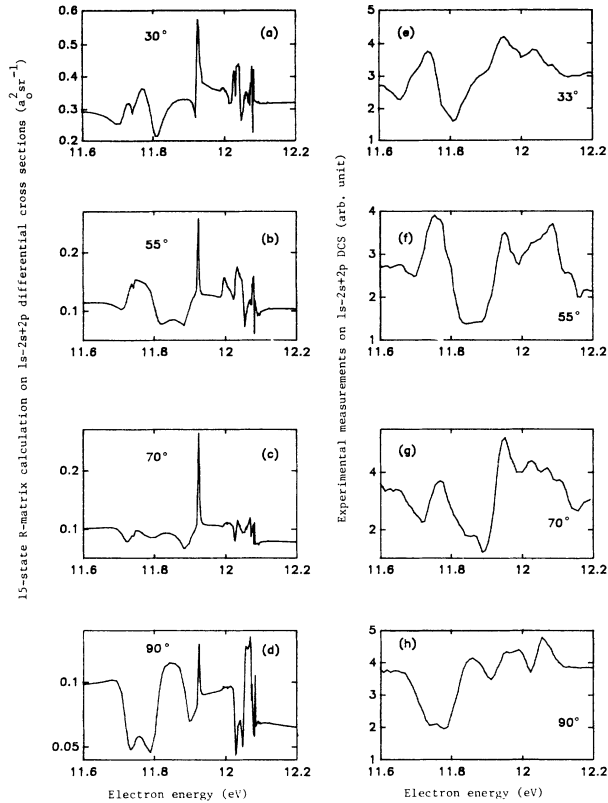


FIG. 7. The $1s \rightarrow 2s + 2p$ differential cross sections as a function of incident electron energy. (a)–(d) the 15-state R -matrix results ($a_0^2 \text{sr}^{-1}$); (e)–(h) the measurements of Warner, Rutter, and King [6] (arbitrary units).

tion of ${}^3F^o$ resonance, which is in good agreement with the experiments. However, the absence of the ${}^3F^o$ peak might lead us to suggest that the abrogation of ${}^{2S+1}F^\pi$ resonance at scattering angle 90° was due to the reason given in Table I. The present 15-state calculation and those of Callaway [28] show unmistakably that the sharp peak does exist at the energy position of the ${}^3F^o$ resonance. This suggests that the calculation of Morgan, McDowell, and Callaway [7] did not have enough energy points to map out the actual shape of the resonant profile and its agreement with the experiments [6] is purely by coincidence.

D. The spin asymmetry $A_{1s \rightarrow 2s}(\theta, k^2)$

The spin asymmetry is defined by Eq. (2). If we drop the subscripts i and j , we have

$$A = (1-r)/(1+3r), \quad (5)$$

where r is the ratio of the triplet cross section to the singlet in the $1s \rightarrow 2s$ transition. With this definition, $A=1$ corresponds to pure singlet scattering while $A=-\frac{1}{3}$ represents pure triplet scattering. Hence, in general, the value of A should vary between 1 and $-\frac{1}{3}$.

Figure 8 shows the spin asymmetry $A_{1s \rightarrow 2s}(\theta, k^2)$ as a function of scattering angle θ with fixed energy k^2 . At incident electron energy ranging from $n=2$ to 3 thresh-

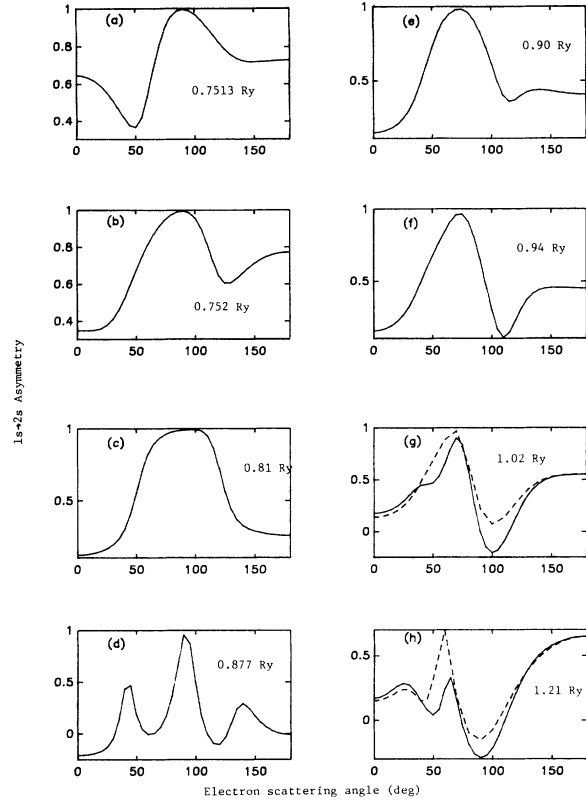


FIG. 8. The 15-state R -matrix calculation for the spin asymmetry $A_{1s \rightarrow 2s}(\theta, k^2)$ as a function of electron scattering angles at electron energies (a) 0.7513 Ry; (b) 0.752 Ry; (c) 0.810 Ry; (d) 0.877 Ry; (e) 0.90 Ry; (f) 0.94 Ry; (g) 1.02 Ry; and (h) 1.21 Ry. —, the present 15-state R -matrix results; - - -, the 6CCO calculation [29].

old [see Figs. 8(a)–8(d)], the general feature of the spin asymmetry $A_{1s \rightarrow 2s}(\theta, k^2)$ takes the shape as shown in Fig. 8(c) at nonresonant region such as $k^2=0.81$ Ry; single maximum at around 90° , bell shape. However, at $k^2=0.7513$ and 0.877 Ry [see Figs. 8(a) and 8(d)], the shapes of the $1s \rightarrow 2s$ asymmetry deviate from Fig. 8(c). These energies correspond to the ${}^1P^o$ shape resonance and the ${}^3F^o$ Feshbach resonance. The shapes take the form of the inverse of $\{P_1(\cos\theta)\}^2$ and $\{P_3(\cos\theta)\}^2$ with the maximum value at 1 and minimum value $-\frac{1}{3}$.

Figures 8(e)–8(h) show the progressive evolution of the shape for the spin asymmetry $A_{1s \rightarrow 2s}(\theta, k^2)$ as a function of electron scattering angle at nonresonance energies. As incident electron energy increases from 0.90 to 1.21 Ry, two small maxima at smaller angles and a deep minimum at larger angle are slowly evolved. The general shape of the spin asymmetry at energies 1.02 and 1.21 Ry is confirmed by the 6CCO calculation of Bray, Konovalov, and McCarthy [29] [see Figs. 8(g) and 8(h)].

In our previous paper [10] it was reported that the 15-state R -matrix calculation on the elastic spin asymmetry $A_{1s \rightarrow 1s}(\theta, k^2)$ is extremely sensitive to the presence of resonances and that at scattering angle 90° , the qualitative shapes of the profiles belonging to the $A_{1s \rightarrow 1s}(\theta, k^2)$ parameter and elastic differential cross section show re-

markable resemblance to each other. It is interesting to investigate the sensitivity of the spin asymmetry for the inelastic $1s \rightarrow 2s$ transition in response to the presence of resonances.

Figure 9 shows the 15-state calculation on $1s \rightarrow 2s$ asymmetry as a function of electron energy as the incident electron energy increases from 0.855 Ry up to $n=3$ threshold at scattering angles 0° and 30° . There is a striking similarity between the structure in the $1s \rightarrow 2s$ spin asymmetry at 0° and 30° . It is attributed to the fact that at these angles, none of the low partial waves is enhanced or suppressed and the effects from the resonances contribute to the $1s \rightarrow 2s$ asymmetry at scattering angle 0° in the same way as they do at scattering angle 30° . It is also noted that the triplet resonances $^3P^o$, $^3F^o$, $^3D^e$, $^3P^o$, $^3P^o$ (the long vertical bars indicated in Fig. 9) lead to a small region of excess triplet scattering. However, the triplet amplitude is reduced below each resonance and enhanced above it; so the negative spin asymmetry is observed not on the resonance but at slightly higher ener-

gies (see Fig. 9).

Figure 10 compares the 15-state R -matrix calculation on $1s \rightarrow 2s$ DCS with its counterpart on $1s \rightarrow 2s$ asymmetry at scattering angle 90° . The vertical bars represent positions of the resonances given in Table II. The resemblance in structure between the $1s \rightarrow 2s$ differential cross sections and the spin asymmetry is still visible, although it is not as strong as in the case of elastic scattering. The $1s \rightarrow 2s$ asymmetry seems to reach its maximum value 1 at the nonresonant background (i.e., pure singlet scattering). Table III shows the 15-state R -matrix calculation on the T -matrix elements for the $1s \rightarrow 2s$ excitation. It is clear that the singlet scattering dominates the even partial waves while the triplet scattering dominates the odd partial waves at energy 0.81 Ry (which is far from any known resonance). At scattering angle 90° , all the odd partial contributions are removed and hence the triplet scattering effects are suppressed. Subsequently, the $1s \rightarrow 2s$ spin asymmetry value approaches almost to 1. At energy 0.877 Ry which features the $^3F^o$ resonance, a simi-

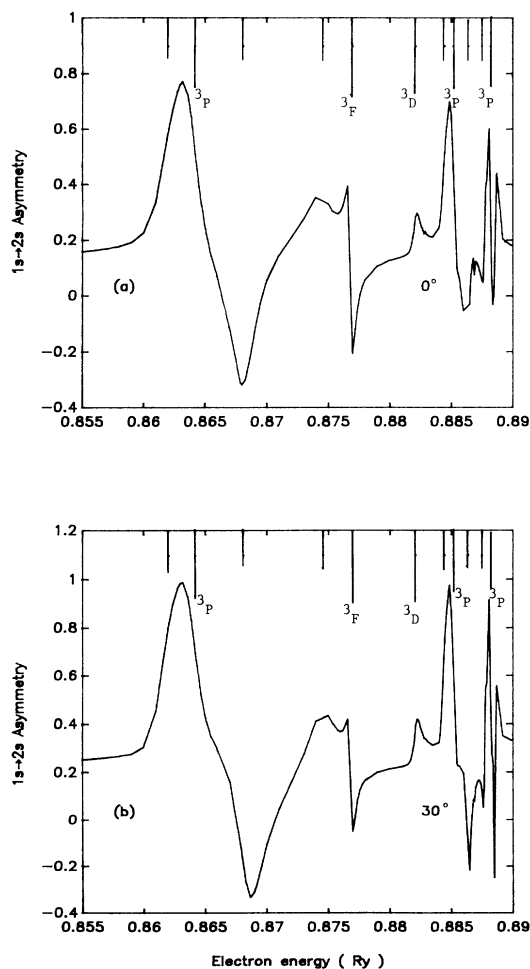


FIG. 9. The 15-state R -matrix calculation for the spin asymmetry $A_{1s \rightarrow 2s}(\theta, k^2)$ as a function of incident electron energy ranging from 0.855 to 0.89 Ry at electron scattering angles (a) 0° ; (b) 30° . The vertical bars indicate positions of the resonances given in Table II in increasing energies.

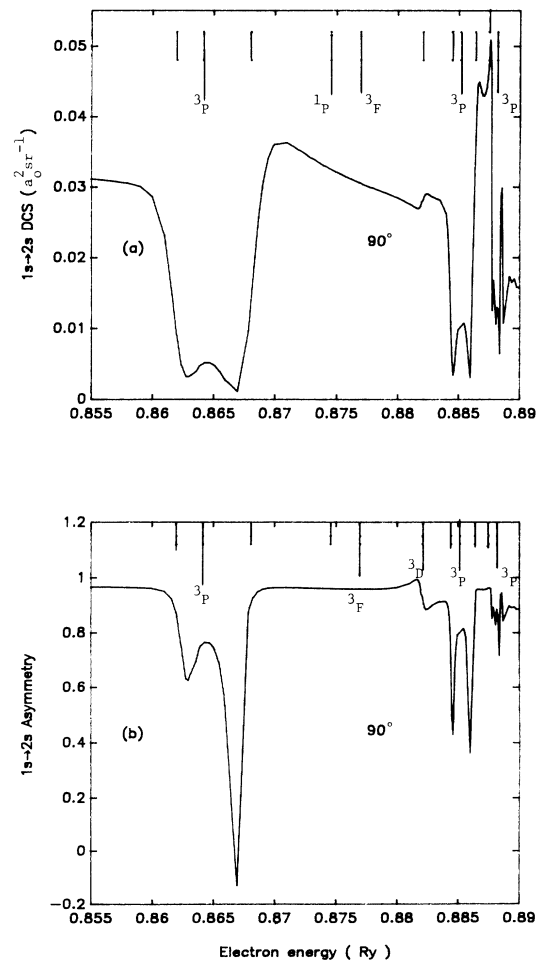


FIG. 10. The 15-state R -matrix calculation on (a) $1s \rightarrow 2s$ differential cross section ($a_0^2 \text{sr}^{-1}$); (b) spin asymmetry $A_{1s \rightarrow 2s}(\theta, k^2)$ as functions of incident electron energy ranging from 0.855 to 0.89 Ry at scattering angle 90° . The vertical bars indicate positions of the resonances given in Table II in increasing energies.

TABLE III. T -matrix elements for the $1s \rightarrow 2s$ transition. (Figures in brackets denote the power of 10 by which the number should be multiplied.)

	0.81 Ry		0.867 Ry		0.877 Ry	
	Real	Imaginary	Real	Imaginary	Real	Imaginary
Singlet						
0	-0.271[0]	-0.371[0]	-0.492[0]	-0.113[0]	-0.434[0]	-0.158[0]
1	0.619[-1]	0.118[-1]	0.110[0]	0.942[-2]	0.538[-1]	-0.284[-1]
2	-0.151[0]	0.127[0]	-0.171[0]	-0.420[-1]	-0.104[0]	0.200[0]
3	0.154[-1]	0.134[-1]	0.318[-1]	0.214[-1]	0.350[-1]	0.230[-1]
4	0.400[-2]	0.307[-2]	0.742[-2]	0.924[-2]	0.664[-2]	0.105[-1]
5	0.844[-3]	0.382[-3]	0.282[-2]	0.146[-2]	0.322[-2]	0.172[-2]
Triplet						
0	0.276[-1]	-0.195[-1]	0.858[-2]	-0.437[-1]	0.499[-2]	-0.463[-1]
1	-0.539[-1]	0.144[0]	0.107[0]	0.152[0]	0.341[-1]	-0.174[0]
2	0.209[-1]	-0.156[-1]	0.372[-1]	-0.210[-1]	0.377[-1]	-0.202[-1]
3	0.231[-2]	0.398[-1]	-0.107[-1]	0.412[-1]	0.196[0]	0.596[-1]
4	0.395[-2]	0.287[-2]	0.909[-2]	0.755[-2]	0.993[-2]	0.842[-2]
5	0.841[-3]	0.379[-3]	0.280[-2]	0.143[-2]	0.319[-2]	0.169[-2]

lar situation prevails: only odd partial waves have appreciable triplet scattering. Large increase in the magnitude of the T matrix in the ${}^3F^o$ partial wave indicates strongly the presence of a ${}^3F^o$ Feshbach resonance (see Table III). At scattering angle 90° , the dominant contribution from the ${}^3F^o$ partial wave is removed together with the other odd partial waves' contribution. The $1s \rightarrow 2s$ spin asymmetry therefore shows no sign of the presence of the ${}^3F^o$ resonance and it merges into the smooth background with the spin asymmetry value almost equal to 1. However, in the vicinity of the ${}^3P^o$ resonance at 0.867 Ry, the dominance of the even partial waves by the singlet scattering and the odd partial waves by the triplet scattering is not observed and it gives rise to a small region of excess triplet scattering immediately above the ${}^3P^o$ resonance (see Table III).

IV. CONCLUSION

A 15-state R -matrix calculation on inelastic differential cross sections for the excitation of the $n=2$ states of atomic hydrogen has been computed at 530 energies and over a wide range of angles to study the feasibility of using the electron-energy-loss experiments in the investigation of resonances. We are satisfied with the following conclusions: (i) The electron-energy-loss experiments do not represent an attractive alternative in the extraction of resonant positions and widths in the inelastic scattering process, as it is lacking in resolution compared to optical techniques; (ii) the mixing of $2p$ contribution in the

$1s \rightarrow 2s + 2p$ DCS profile gives rise to irregular structures which make it impossible to identify the state of the resonances; (iii) further pursuit of the experimental investigation in this direction would not be productive unless the electron-energy-loss experiments are supplemented with the simultaneous measurement of the scattered electron coincident with the $2p$ decay photons.

The present calculation on the angular distribution of the spin asymmetry in the inelastic scattering of spin-polarized electrons by spin-polarized hydrogen atoms for the $1s \rightarrow 2s$ excitation is more sensitive to the presence of resonances than the spin-averaged inelastic differential cross sections.

ACKNOWLEDGMENTS

We would like to thank Professor P. G. Burke, Professor A. E. Kingston, Dr. Pathak, and Dr. K. A. Berrington for their continued interest and support. The majority of these calculations were carried out on the Cray X-MP/48 computer at the SERC Atlas Laboratory, Didcot, United Kingdom. Data analysis was carried out on the UNISYS 1100/61 computer systems at the Computer Centre, University of Malaya, Kuala Lumpur. F.W.C. and K.R. would like to acknowledge financial assistance from University of Malaya Research Funds (Vote F). Finally, we would like to thank Professor J. Callaway, Professor I. E. McCarthy, and Professor J. F. Williams for sending their data in tabular form.

- [1] J. F. Williams, *J. Phys. B* **21**, 2107 (1988).
- [2] J. Callaway, *Phys. Rev. A* **26**, 199 (1982).
- [3] D. Andrick, H. Ehrhardt, and M. Eyb, *Z. Phys.* **214**, 388 (1968).
- [4] W. C. Fon and K. P. Lim, *J. Phys. B* **23**, 3691 (1990).
- [5] J. F. Williams, *J. Phys. B* **9**, 1519 (1976).
- [6] C. D. Warner, P. M. Rutter, and G. C. King, *J. Phys. B*

- 23**, 93 (1990).
- [7] L. A. Morgan, M. R. C. McDowell, and J. Callaway, *J. Phys. B* **10**, 3297 (1977).
- [8] J. F. Williams, *J. Phys. B* **14**, 1197 (1981).
- [9] A. Pathak, A. E. Kingston, and K. A. Berrington, *J. Phys. B* **21**, 2939 (1988); A. Pathak, P. G. Burke, and K. A. Berrington, *ibid.* **22**, 2759 (1989).

- [10] W. C. Fon, K. M. Aggarwal, and K. Ratnavelu, *J. Phys. B* **25**, 2625 (1992); W. C. Fon, K. Ratnavelu, and K. M. Aggarwal, *Phys. Rev. A* **47**, 2968 (1993).
- [11] P. G. Burke, A. Hibbert, and W. D. Robb, *J. Phys. B* **4**, 153 (1971).
- [12] K. A. Berrington, P. G. Burke, M. Le Dourneuf, W. D. Robb, K. T. Taylor, and Vo Ky Lan, *Comput. Phys. Commun.* **14**, 367 (1978).
- [13] K. M. Aggarwal, K. A. Berrington, P. G. Burke, A. E. Kingston, and A. Pathak, *J. Phys. B* **24**, 1385 (1991).
- [14] M. Gailitis and R. Damburg, *Zh. Eksp. Teor. Fiz.* **44**, 1644 (1963) [*Sov. Phys. JETP* **17**, 1106 (1963)].
- [15] M. Gailitis and R. Damburg, *Proc. Phys. Soc. London* **82**, 192 (1963).
- [16] L. Lipsky, R. Anania, and M. J. Conneely, *At. Data Nucl. Data Tables* **20**, 127 (1977).
- [17] R. S. Oberoi, *J. Phys. B* **5**, 1120 (1972).
- [18] Y. K. Ho and J. Callaway, *Phys. Rev. A* **27**, 1187 (1983).
- [19] Y. K. Ho and J. Callaway, *Phys. Rev. A* **34**, 130 (1986).
- [20] The results can be obtained in printed form or via electronic mail at the address j2kurun@fileservr.cc.um.MY
- [21] P. G. Burke, S. Ormonde, and W. Whitaker, *Phys. Rev. Lett.* **17**, 800 (1966); *Proc. Phys. Soc. London* **92**, 319 (1967).
- [22] A. J. Taylor and P. G. Burke, *Proc. Phys. Soc. London* **92**, 336 (1967).
- [23] K. A. Berrington and A. E. Kingston, *J. Phys. B* **20**, 6631 (1987).
- [24] T. T. Scholz, H. R. J. Walters, and P. G. Burke, *Mon. Not. R. Astron. Soc.* **242**, 692 (1990).
- [25] I. E. McCarthy and Bo Shang, *Phys. Rev. A* **46**, 3959 (1992).
- [26] W. C. Fon, K. P. Lim, and P. M. J. Sawey, *J. Phys. B* **26**, 305 (1993).
- [27] I. Bray and I. E. McCarthy, *Phys. Rev. A* **47**, 317 (1993).
- [28] J. Callaway, *J. Phys. B* **23**, 751 (1990).
- [29] I. Bray, D. A. Konovalov, and I. E. McCarthy, *Phys. Rev. A* **44**, 5586 (1991).